Optical Materials 36 (2014) 1525–1533

Contents lists available at ScienceDirect

Optical Materials

journal homepage: www.elsevier.com/locate/optmat

Improvement of intramolecular charge transfer within a donor–acceptor blend by doping novel synthesized benzothiadiazole small molecules in solid state

Haluk Dinçalp [a,*], Gözde Murat [a], Sıddık İçli [b]

[a] Department of Chemistry, Faculty of Arts and Science, Celal Bayar University, Muradiye 45030, Manisa, Turkey
[b] Solar Energy Institute, Ege University, Bornova 35100, Izmir, Turkey

ARTICLE INFO

Article history:
Received 29 November 2013
Received in revised form 30 March 2014
Accepted 15 April 2014
Available online 9 May 2014

Keywords:
Benzothiadiazole
Organic photovoltaic
Time resolved emission spectra
Solid state emission
Charge-separation

ABSTRACT

Three electron-deficient small molecules based on 2,1,3-benzothiadiazole (BTD) units namely, 4,7-bis (3-methoxyphenyl)-2,1,3-benzothiadiazole (**BT1**), (3-{7-[3-(dimethylamino)phenyl]-2,1,3-benzothiadiazole-4-yl}phenyl)dimethylamine (**BT2**) and 3,3′-(2,1,3-benzothiadiazole-4,7-dyl)dianiline (**BT3**) were synthesized and their photophysical properties were investigated systematically to understand their potential usage in ternary organic solar cells (OSCs) as additive material to enhance the cell efficiency. All these molecules show broad absorption bands in 350–750 nm on glass substrate and their optical band gaps were calculated to be around 2.50–2.80 eV. BTD fluorescence dynamics were measured in polymer:BT1:fullerene blends with varying emission wavelengths of active layer. Fluorescence emission and time resolved measurements indicated photoinduced energy shift from **BT1** dye to fullerene and also from polymer to **BT1** dye upon excitation of the active layer.

1. Introduction

New family of organic semiconductors is in progress for the development of cheap and high performance photovoltaic materials. Polymers containing 2,1,3-benzothiadiazole (BTD) units have been successfully used in organic solar cells (OSCs). One of these, poly[2,6-(4,4-bis-(2-ethylhexyl)-4H-cyclopenta[2,1-b;3,4-b′]-dithiophene)-alt-4,7-(2,1,3-benzothiadiazole)] [PCPDTBT], in blends with [6,6]-phenyl C_{71}-butyric acid methyl ester ($PC_{71}BM$), has been reported as giving satisfyingly a high power conversion efficiency (PCE) of 3.2% and external quantum efficiency of 38% [1]. Cell efficiency of bulk-heterojunction solar cells (BHJCs) based on poly(3-hexylthiophene) (P3HT)/[6,6]-phenyl C_{61}-butyric acid methyl ester ($PC_{61}BM$) blends has been enhanced by the addition of small fractions of PCPDTBT polymer and efficiency has been reached to a value of 2.8% [2]. Efficient BHJCs have been fabricated using a benzothiadiazole-thiophene co-polymer, PCDTPT, in blends with PCBM giving impressive performances with PCE values around 6.0–6.5% [3,4].

BTDs are one of the most used groups in conjugated systems because of their high fluorescence activity, efficient electron-withdrawing capacity, well-ordered crystal structures and high reduction potentials [5]. Many groups have preferred the BTD containing polymers or co-polymers blending with different mass ratios of PCBM acceptor to fabricate efficient OSC devices [6–13]. BTD units in these polymers contribute the cell performance by lowering the band gap and improving the absorption covering the entire solar spectra [14,15]. Also, small molecule BTD derivatives play an important role in OSC technologies. As compared to the polymeric counterparts, many of small molecules have well-defined molecular structures and are easy to re-synthesize, functionalize and purify [16]. There are several families of solution processable BTD small molecules that have been used as donor materials in BHJ solar cells in literature [17–28]. Among these studies, Wang and co-workers have reported a promising result with an impressive V_{oc} of 1.04 V and a PCE of 3.85% by fabricating a device with blended $PC_{61}BM$ and BTD-triphenylamine type small molecule [29]. Horie and co-workers have used a BTD/cyclopentadithiophene small molecule as a sensitizer in a ternary blend with classical P3HT:$PC_{61}BM$ type OSCs and obtained a high cell efficiency value of 4.1% [30].

Detailed analysis of photophysical process within donor and acceptor sites in blend is necessary to clarify the charge transfer contribution of BTD small molecule to overall performance for these OSC devices described above. P3HT:$PC_{61}BM$ blends have granted a convenient model to understand the photophysics and charge generation dynamics in many donor–acceptor groups in

* Corresponding author. Tel.: +90 236 2013158; fax: +90 236 2412158.
E-mail address: haluk.dincalp@cbu.edu.tr (H. Dinçalp).

http://dx.doi.org/10.1016/j.optmat.2014.04.019
0925-3467/

OSC devices [31–35]. In these systems, it is known that excitons are conveyed to the interface, where they separated into charge carriers, by charge transfer from donor P3HT to acceptor PCBM. In a ternary system, where one component (BTD small molecule) acts as sensitizer and the others as charge transporting system components (P3HT/$PC_{61}BM$). BTD contribution to overall charge shift has not been discussed yet. Samuel and co-workers have investigated the singlet exciton diffusion and decay dynamics in conjugated PCDTPT polymers blended with fullerene acceptor. They have reported that exciton diffusion occurs into the polymer inside at very low concentrations of fullerene, whereas Förster-type energy transfer to the fullerene is the main process at higher fullerene concentrations [36].

In this report, we have managed to synthesize three kinds of new BTD derivatives with different donor substituents, as shown in Fig. 1. Also, we have focused on photoinduced energy or electron transfer process between donor and acceptor components in P3HT:BTD:$PC_{61}BM$ ternary structure using fluorescence emission and time resolved measurements. We have compared the photophysical properties of BTD dyes on thin films with in solutions of different polarities.

2. Experimental section

2.1. General procedures

^1H NMR and ^{13}C NMR were performed using a Bruker 400 MHz spectrometer. FT-IR spectra were carried out using a Perkin Elmer-Spectrum BX spectrophotometer preparing KBr pellets. UV–vis spectra were recorded using a UV–vis–NIR spectrometer (Perkin Elmer Lambda 950) in solutions and on thin films. Fluorescence and life time measurements were obtained using a FLSP 920 Edinburg fluorescence phosphorescence spectrophotometer. The fluorescence life times were determined by the single photon timing method using a laser which has been used to excite the samples at 472 nm. The Edinburgh Instruments F900 exponential tail fit method [37] was used for calculations. Single photon timing method was used to obtain the fluorescence decay histograms in 10,000 data channels. The fitted decay curve was settled by the fitting parameters such as $\chi^2 < 1.2$ goodness of fit. The instrument response function (IRF) was determined using a ludox scattering solution.

To investigate the electrochemical characteristics of synthesized **BT1-3** dyes, cyclic voltammetry (CH instruments-Electrochemical Workstation) measurements were performed with a standard three-electrode electrochemical compartment in 100 mM [TBA][PF6] solution in Me–CN as the supporting electrolyte. Ag/AgCl, glassy carbon and Pt wire electrodes were used as reference, working and counter electrodes, respectively. The scan rate was at 50 mV/s. Ferrocene–ferrocenium (Fe/Fe^+) couple which was exhibited at about +0.55 V was used as internal reference for the calculation of the onset values of E_{red}. HOMO and LUMO energy levels of **BT1-3** dyes were calculated by the formulas [38]:

$$E_{LUMO} = -(4.8 + E_{red}^{onset}),\quad E_{red}^{onset} = E_{red}^{0} - E_{ox(ferrocene)}^{0},\quad E_{HOMO} = E_{LUMO} - E_{gap}$$

$PC_{61}BM$ and other photoactive components were dissolved at concentrations of 1 wt% from *o*-dichlorobenzene (oDCB) solution in different mass ratios. Active layer was coated onto the glass surface by spinning and, then the coated substrate was dried at 75 °C for 30 min under vacuum.

2.2. Materials

Chloroform, silica gel, *tetrakis*(triphenylphosphine)palladium(0), hydrogen bromide solution (47%) were purchased from Merck Company. Benzene, sodium carbonate, bromine were purchased from Carlo Erba. Ethanol, 2,1,3-benzothiadiazole, magnesium sulfate, 3-(*N,N*-dimethylamino)-phenylboronic acid, 3-aminophenylboronic acid hemisulfate were purchased from Sigma–Aldrich. 3-methoxybenzeneboronic acid (from Alfa Aesar) and $NaHSO_3$ (Riedel-de-Haën) were used as received. Other organic solvents were analytical grade and used without further purification.

2.3. Synthesis

2.3.1. Synthesis of 4,7-dibromo-2,1,3-benzothiadiazole (*BT*) [39]

To a 250 mL two-necked round bottom flask were added benzothiadiazole (2 g, 14.7 mmol) and 30 mL of HBr (47%). A solution containing Br_2 (10.17 g, 63.6 mmol) in 20 mL of HBr was added dropwise for 1 h. After total addition of the Br_2, the solution was refluxed at 120 °C for 6 h. Precipitation of an orange solid was noted. The mixture was allowed to cool to room temperature and sufficient saturated solution of $NaHSO_3$ was added to consume completely any excess Br_2. The mixture was filtered under vacuum and washed exhaustively with water. The solid was then washed once with cold Et_2O and dried under vacuum, affording the desired

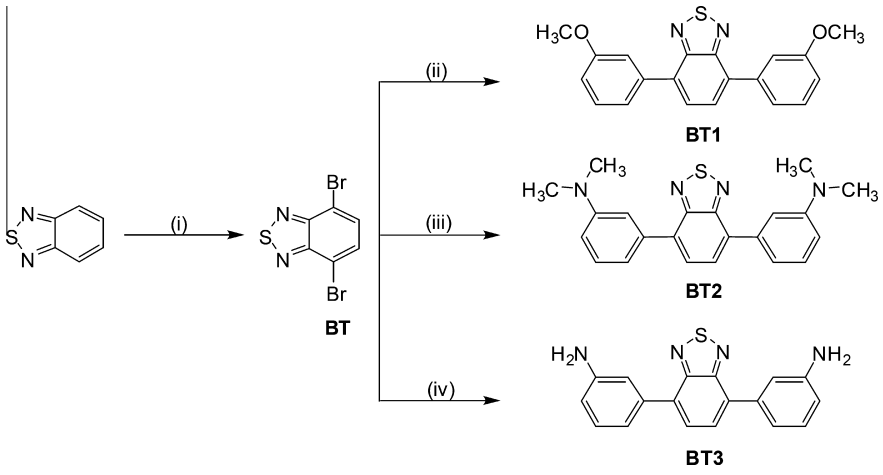

Fig. 1. Synthetic pathways of the studied molecules. (i) Br_2/HBr, 120 °C, 93%; (ii) 3-methoxybenzene boronic acid, Na_2C0_3, ethanol/benzene, $Pd(PPh_3)_4$, 85 °C, 85%; (iii) 3-(N,N-dimethylamino)phenyl boronic acid, Na_2C0_3, ethanol/benzene, $Pd(PPh_3)_4$, 85 °C, 84%; (iv) 3-aminophenyl boronic acid hemisulfate, Na_2C0_3, ethanol/benzene, $Pd(PPh_3)_4$, 85 °C, 75%.

dibrominated product in 95% yield. FT–IR (KBr pellet, cm^{-1}): 3016 and 2970 (aromatic ν_{C-H}), 1739, 1586 (aromatic $\nu_{C=C}$), 1476, 1365, 1309, 1217, 1184, 936, 875, 824, 586, 527, 487 cm^{-1}. ^1H NMR (400 MHz, $CDCl_3$, δ 7.26 ppm): δ = 7.71 (2H, s), ^{13}C NMR [100 MHz, DMSO δ 40.22 (7 peaks)]: δ = 152.9, 133.4, 113.7 ppm.

2.3.2. General procedure for the synthesis of Suzuki coupling reactions [40]

To boronic acid derivatives (2 equiv.) in ethanol was added a mixture of dibrominated product (1 equiv.) in benzene and aqueous 2 M sodium carbonate solution under an argon atmosphere. Subsequently, *tetrakis*(triphenylphosphine)palladium(0) (≈5.33%) was added to the mixture at 60 °C. After the mixture was heated at 85 °C for 15 h under an argon atmosphere, the reaction mixture was poured into water and extracted with chloroform. The organic layer was dried over anhydrous magnesium sulfate and evaporated in vacuum to dryness. The residue was separated by column chromatography on silica gel (*n*-hexane:ethyl acetate 4:1 (v/v)).

*2.3.3. Synthesis of 4,7-bis(3-methoxyphenyl)-2,1,3-benzothiadiazole (**BT1**)*

Dibrominated product (0.096 g, 0.330 mmol) in benzene (40 mL), 2 M Na_2CO_3 (18 mL), 3-methoxybenzeneboronic acid (0.1 g, 0.660 mmol) in ethanol (10 mL) and *tetrakis*(triphenylphosphine)palladium(0) (0.0200 g, 0.0176 mmol) were used and synthesized according to the general procedure. Yield 85%. FT–IR (KBr pellet, cm^{-1}): 2924 and 2854 (aliphatic ν_{C-H}), 1738, 1604, 1578 (aromatic $\nu_{C=C}$), 1474, 1344, 1292, 1226, 1042, 844, 778, 694, 564 cm^{-1}. ^1H NMR (400 MHz, $CDCl_3$ δ 7.24 ppm): δ = 7.76 (2H, s), 7.52 (4H, d, J = 11.0 Hz), 7.44 (2H, t, J = 7.7 Hz), 7.00 (2H, dd, J_1 = 7.7 Hz J_2 = 3.6 Hz), 3.89 (6H, s) ppm. ^{13}C NMR [100 MHz, $CDCl_3$ δ 77.2 (3 peaks)]: δ = 159.9, 154.2, 138.9, 133.4, 129.8, 128.2, 121.8, 115.3, 114.0, 55.5 ppm.

*2.3.4. Synthesis of (3-{7-[3-(dimethylamino)phenyl]-2,1,3-benzothiadiazole-4-ly}phenyl)dimethylamine (**BT2**)*

Dibrominated product (0.089 g, 0.303 mmol) in benzene (35 mL), 2 M Na_2CO_3 (24 mL), 3-(*N*,*N*-dimethylamino)-phenylboronic acid (0.1 g, 0.606 mmol) in ethanol (10 mL) and *tetrakis*(triphenylphosphine)palladium(0) (0.0186 g, 0.0162 mmol) were used and synthesized according to the general procedure. Yield 84%. FT–IR (KBr pellet, cm^{-1}): 3076, 2922 and 2806 (aliphatic ν_{C-H}), 1598 (aromatic $\nu_{C=C}$), 1502, 1434, 1374, 1236, 1180, 1002, 942, 844, 762, 692 cm^{-1}. ^1H NMR (400 MHz, $CDCl_3$ δ 7.25 ppm): δ = 7.77 (2H, s), 7.40 (2H, d, J = 7.7 Hz), 7.31 (2H, s), 7.26 (2H, s), 6.84 (2H, dd, J_1 = 7.7 Hz J_2 = 2.6 Hz), 3.02 (12H, s) ppm. ^{13}C NMR [100 MHz, $CDCl_3$ δ 77.2 (3 peaks)]: δ = 154.5, 151.0, 138.5, 134.3, 129.4, 128.2, 118.0, 113.9, 112.8, 40.9 ppm.

*2.3.5. Synthesis of 3,3′-(2,1,3-benzothiadiazole-4,7-dyl)dianiline (**BT3**)*

Dibrominated product (0.079 g, 0.269 mmol) in benzene (33 mL), 2 M Na_2CO_3 (16 mL), 3,3′-aminophenylboronic acid hemisulfate (0.1 g, 0.538 mmol) in ethanol (9 mL) and *tetrakis*(triphenylphosphine)palladium(0) (0.0165 g, 0.0144 mmol) were used and synthesized according to the general procedure. Yield 75%. FT–IR (KBr pellet, cm^{-1}): 3426, 3342 (stretching ν_{N-H}), 3190, 2924, 2852, 1720, 1604, 1584 (aromatic $\nu_{C=C}$), 1478, 1350, 1246, 1122, 850, 784, 700, 504 cm^{-1}. ^1H NMR (400 MHz, DMSO δ 2.48 ppm): δ = 7.79 (2H, s), 7.18–7.14 (4H, m), 7.07 (d, 2H, J = 7.7 Hz), 6.65 (2H, d, J = 7.7 Hz), 5.17 (4H, s) ppm. ^{13}C NMR [100 MHz, DMSO δ 39.7 (7 peaks)]: δ = 154.1, 149.1, 138.2, 133.5, 129.7, 128.6, 117.8, 115.3, 114.8 ppm.

3. Results and discussion

3.1. Optical properties and CV measurements

Fig. 2a shows the UV–vis absorption spectra of **BT2** dye in four different solvents of polarities and Fig. 2b gives the comparison of

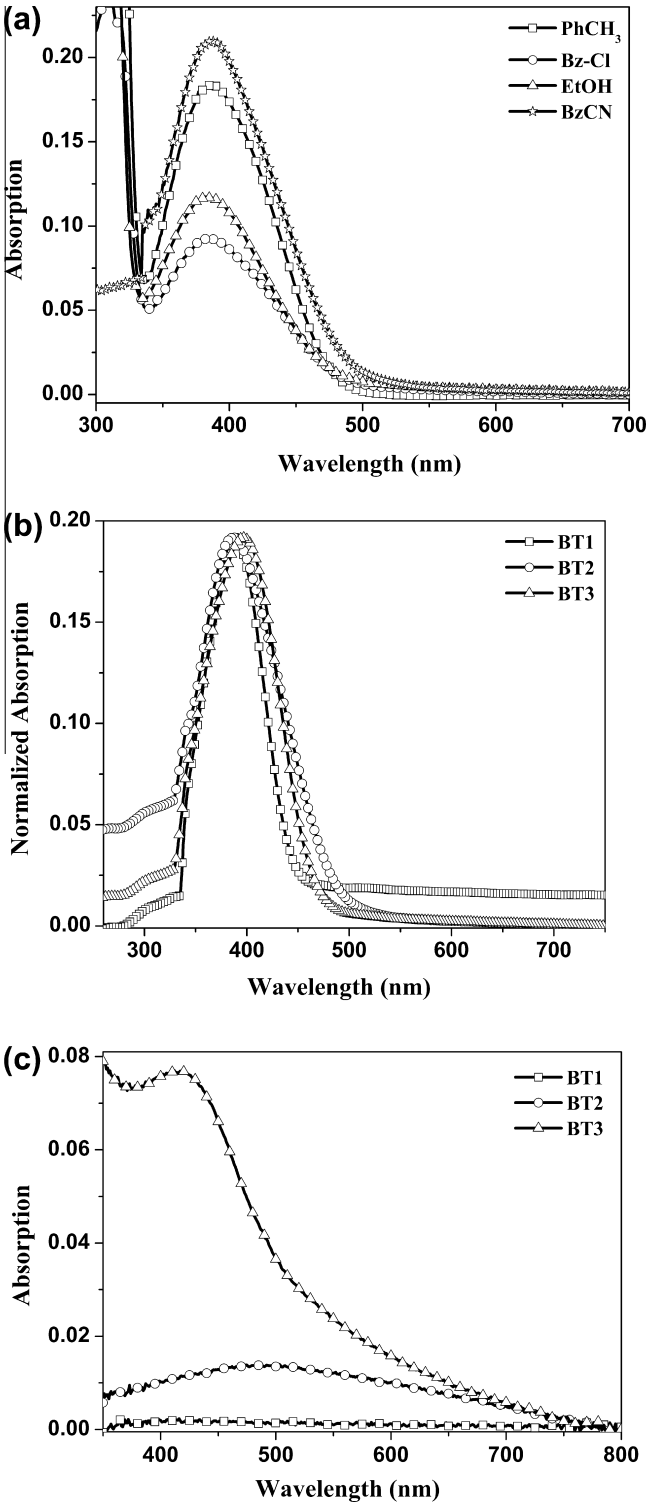

Fig. 2. (a) UV–vis absorption spectra for **BT2** dye in four different solvents of polarities, and (b) normalized UV–vis absorption spectra for **BT1-3** dyes in Bz–CN solutions at the concentrations of 6.6×10^{-5} M. (c) Solid state UV–vis absorption spectra for **BT1-3** dyes on thin films.

UV–vis absorption spectra of **BT1-3** dyes in Bz–CN solution, and the corresponding optical properties are summarized in Table 1. The absorption spectra of **BT1-3** dyes illustrate typical transitions bands in the wavelength region of 350–500 nm assigned to the π–π^* transition, which predominantly originates in HOMO−LUMO excitations. The absorption maximum of **BT3** dye is slightly shifted to red region in Bz–CN because of the enhanced n–π^* transition supported by the non-bonding electrons of amine groups attached to phenyl rings. All of the dyes give little hypsochromic shifts of 3–4 nm in ethanol compared to the corresponding spectra in other solvents. This observation is ascribed to lower polarizabilities of excited states for the studied dyes in ethanol.

Solid-state optical properties of **BT1-3** compounds are illustrated in Fig. 2c. On thin films, **BT1-3** dyes form a molecular-packed form of π-conjugated aromatic structure so that the absorption spectra give broader and more red-shifted absorption bands with relative to those in solutions, as known from the literature for similar reports [41,42]. However, **BT1** dye has shown the worst coating property on thin films among the other studied dyes. This behavior may be attributed to the weak interaction between the functional group of the dye and SiO_2-based glass substrate, leading the formation of small aggregates on the substrate surface. Also, Fig. 2c shows that **BT3** dye illustrates less red-shifted band than that of the other dyes in the solid-state film. This is likely caused by the distortion of intermolecular packing on the film morphology. Intramolecular hydrogen bond formation between the hydrogen atoms of amine group and non-bonding electrons of heteroatoms in aromatic **BT3** dye may form a twisted structure inhibiting the overlap of the aromatic cores properly. As a result, decrease in π-conjugated aromatic bulks causes blue shift in spectra.

Fig. 3a shows steady-state fluorescence spectra of **BT1** in less polar (toluene and chlorobenzene) and more polar (ethanol and benzonitrile) solutions with excitation wavelength of 350 nm. The fluorescence signals for **BT1** dye in $PhCH_3$ and Bz-Cl appeared at 492 and 499 nm, respectively. In EtOH and BzCN solutions, the fluorescence peaks of **BT1** shifted to 516 and 503 nm, respectively, with decreasing fluorescence quantum yields, as shown in Table 1. These solvatochromic behaviors for **BT1** dye may be assigned to the formation of charge transfer (CT) complex. The more efficient excited-state solvatochromic effects were observed for compounds **BT2** and **BT3** dyes in less polar $PhCH_3$ and Bz–Cl solvents. **BT2** compound shows a marked red shift of emission maximum from 448 nm in BzCN to 649 nm in Bz–Cl. Similar red shift from 448 nm in BzCN to 569 nm in Bz–Cl is detected for **BT3** compound at the excitation wavelength of 350 nm. These clearly indicate that **BT2** and **BT3** dyes posses strong intramolecular photoinduced charge transfer from the donor (aniline) to the acceptor (BTD) units. Such large shifts of the emission spectra to longer wavelengths in different solvent of polarities are explained by the formation of CT complex between the donor and acceptor sites of BTD structures [44,45]. Fig. 3b gives a comparison of the emission wavelengths of **BT1-3** dyes in BzCN solutions. It is obvious that

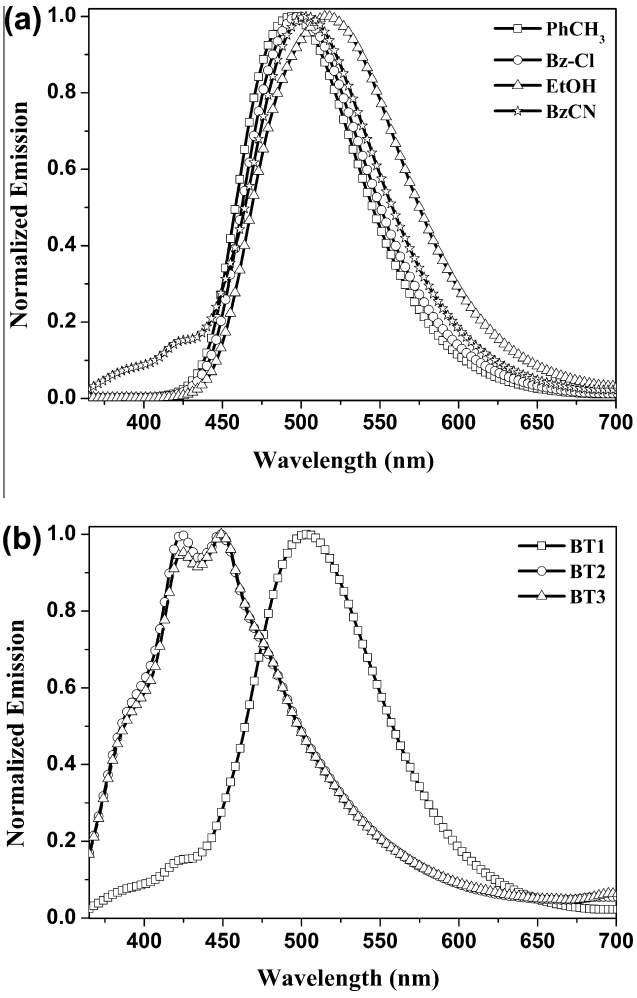

Fig. 3. Normalized fluorescence emission spectra for (a) **BT1** compound in four different solvents of polarities and (b) **BT1-3** compounds in Bz–CN solutions at the concentrations of 6.6×10^{-5} M (λ_{exc} = 350 nm).

excited state of **BT1** has been stabilized by polar BzCN solvent and then a gradual red shift could be observed. However, **BT2** and **BT3** dyes could give emission maxima at lower wavelength of 448 nm because of solvent quenching process between the donor aniline groups and acceptor BzCN solvent molecules. For this reason, CT character from aniline group to BTD center is relatively weak. When the BzCN solvent is replaced by EtOH, the solvatochromic effect is greater than that of BzCN solvent for the studied dyes. Because hydrogen bonding ability of EtOH with the unshared electron pairs of the nitrogen atom enhances CT by donating a partial positive charge into the functional group. Also lower fluorescence quantum yields for **BT2** and **BT3** dyes in all organic solvents around, Φ_F:0.001–0.2 support the efficient CT behavior

Table 1
The maximum wavelength of absorptions and fluorescence emissions (λ (nm)), and fluorescence quantum yields[a] of **BT1-3** dyes in solvents of different polarities (λ_{exc} = 350 nm).

Dyes	Solvents											
	Toluene			Chlorobenzene			Ethanol			Benzonitrile		
	λ	λ_{em}	Φ_F	λ	λ_{em}	Φ_F	λ	λ_{em}	Φ_F	λ	λ_{em}	Φ_F
BT1	387	492	0.92	387	499	0.81	382	516	0.75	387	503	0.31
BT2	386	612	0.10	384	649	0.04	383	483	0.001	386	448	0.03
BT3	396	550	0.20	396	569	0.17	392	488	0.003	396	448	0.03

[a] Fluorescence quantum yields have been determined using quinine sulfate dihydrate (λ_{exc} = 350 nm, Φ_F = 0.577, 0.1 N H_2SO_4) [43].

of the compounds. Free electrons on nitrogen atoms cause intramolecular electron transfer to LUMO level of BTD, which reduces emission intensity.

Table 2 gives us some important physical parameters to understand CT complex in the studied molecules. Fluorescence rate constants of **BT1** dye in $PhCH_3$ and BzCN are higher than that of **BT2** and **BT3** dyes. This means that HOMO level of **BT1** dye is below the HOMO levels of **BT2** and **BT3** dyes in $PhCH_3$ and BzCN solutions, leading to less efficient photoinduced CT for **BT1** dye. Also, observation of the longest components obtained using single-photon-counting system at the excitation wavelength of 350 nm supports a reaction from charge-separated state to the locally excited state for **BT1-3** dyes in $PhCH_3$ and BzCN, as given in Table 2. In $PhCH_3$, the longest components for **BT1-3** dyes around 8–9 ns with major contributions are interpreted in terms of an emission from intramolecular CT complex structure, leading to a delayed fluorescence component. The bathochromic shift of steady-state emission spectra for **BT2** and **BT3** dyes in $PhCH_3$ are responsible for existence of this excited state complex possibly mixed with excited state emission of the dyes. In BzCN, major contribution of 67.8% at the longest decay time of 10.51 ns for compound **BT1** supports the possible formation of CT state. The decay components around 3–4 ns are contributed to the excited fluorescence state of the structures in BzCN solutions. These data are good agreement with that found for thiophene linked BTD small molecule [46]. Also, sub-nanosecond components can be attributed to the existence of an emission from a twisted excited state form of the rings. This conformational change may be due to an interaction between the thiadiazole heteroatoms and donor subunits of phenyl rings.

UV–vis and fluorescence emission spectra for **BT1** and **BT2** dyes on thin films are compared in Fig. 4a and b, respectively. While **BT1** dye has an emission maximum at 502 nm, **BT2** dye shows a major band at 606 nm and a blue-shifted shoulder at 480 nm. This remarkable difference of 104 nm in their emission maxima is assigned to the formation of efficient CT complex in **BT2** dye. Also, no obvious emission signal has been detected for **BT3** dye in thin films due to its strong intramolecular self-quenching process.

Fig. 5 gives the cyclic voltammogram of **BT1-3** dyes and reduction/oxidation peak values are given in Table 3. Compound **BT1** exhibits two reduction waves ($E^0_{red1} = -1.21$ and $E^0_{red2} = -1.45$ V) and two oxidation waves ($E^0_{ox1} = 1.71$ and $E^0_{ox2} = 1.82$ V) indicating the formation of stable anions, dianions, cations and dications of BTD, respectively. When the methoxy group was replaced by the aniline groups, the oxidation potentials of **BT2** and **BT3** compounds reduce to lower value observed at 1.02 and 1.35 V, respectively. The easy oxidation of **BT2** and **BT3** dyes are contributed to more electron releasing capacity of aniline group. LUMO energy levels are calculated from the reduction onset values are calculated to be about −3.04, −3.08 and −3.05 eV for **BT1**, **BT2** and **BT3** dyes, respectively. The lowest HOMO level was found to be about −5.84 eV for **BT1** dye and the order of HOMO levels of the compounds are well-correlated with the fluorescence rate constants given in Table 2.

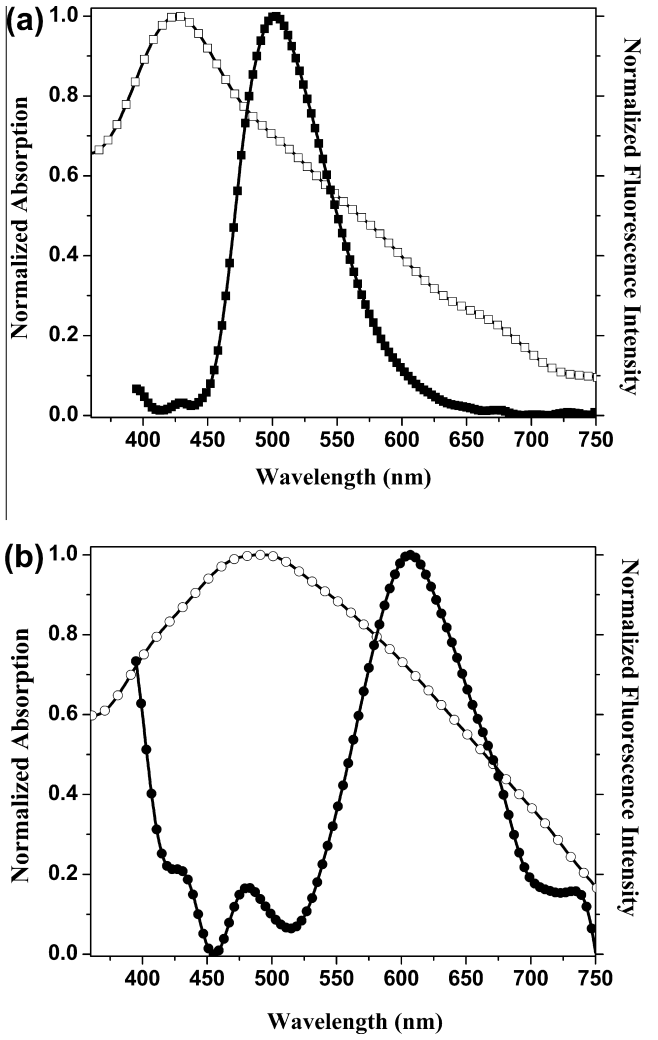

Fig. 4. Comparison of normalized UV–vis and fluorescence emission spectra for (a) **BT1** and (b) **BT2** dyes on thin films (λ_{exc} = 385 nm).

3.2. UV–vis, fluorescence and time resolved measurements on thin films

In order to evaluate the charge transfer contribution of BTD small molecule to overall electron transfer process in

Table 2
Fluorescence decay times (τ_f (ns)) and associated relative amplitudes (α_i (%))[a], fluorescence lifetimes (τ_f (ns)), radiative lifetimes (τ_0 (ns)), fluorescence rate constants ($k^r_f \times 10^7$ (s^{-1})), non-radiative rate constants ($k^{nr} \times 10^8$ (s^{-1})), and singlet energies (E_s (kcal mol^{-1})) of **BT1-3** dyes in toluene and benzonitrile (λ_{exc} = 350 nm).[b]

Solvents/dyes	$\lambda_{det.}$	$\tau_{f(1)}$	α_1	$\tau_{f(2)}$	α_2	$\tau_{f(3)}$	α_3	τ_f	τ_0	k^r_f	k^{nr}	E_s
$PhCH_3$												
BT1	495	0.18	6.6	8.30	93.4	–	–	4.24	4.6	21.7	0.18	74.9
BT2	550	1.57	5.5	9.48	85.5	–	–	5.53	55.3	1.81	1.63	75.1
BT3	550	0.36	3.2	4.64	16.2	8.07	80.6	4.36	21.7	4.60	1.84	73.2
BzCN												
BT1	505	0.56	6.7	3.85	25.5	10.51	67.8	4.97	16.0	6.23	1.39	74.9
BT2	435	0.08	58.3	3.66	24.5	10.55	17.2	4.76	158	0.62	2.04	75.1
BT3	435	0.11	60.9	3.40	21.0	9.89	18.1	4.47	144	0.69	2.17	73.2

[a] Relative amplitude values, α_i, were calculated with the formula [47]: $W\alpha_i = \tau_i \times P_i / \Sigma\tau_i \times P_i$, where τ_i was the decay time of the compound, and P_i was the number of free parameters in the fit function.

[b] Photophysical parameters are calculated with the formulas [48,49]: $\tau_f = \Sigma\tau_{f(n)}/n$, $\tau_0 = \tau_f/\Phi_F$, $k_f = 1/\tau_f = k^r_f + k^{nr}$, $k^r_f = 1/\tau_0$, $E_s = 0.0029/\lambda_{long} \times 10^{-7}$.

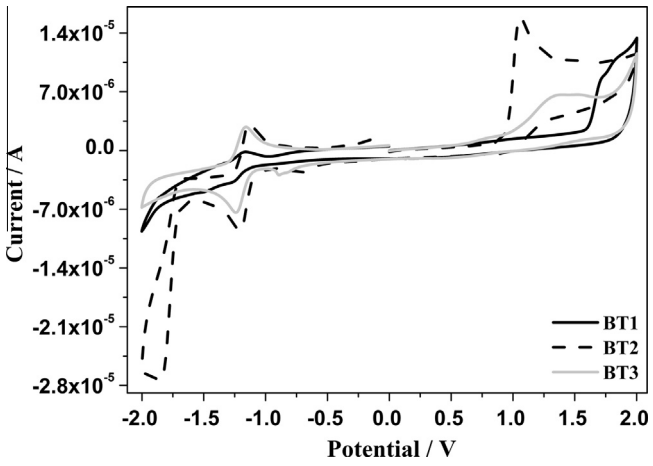

Fig. 5. Comparison of cyclic voltammograms of **BT1-3** compounds on glassy carbon working electrode in 0.1 M [TBA][PF6]/Me–CN (Scan rate: 100 mV s^{-1}).

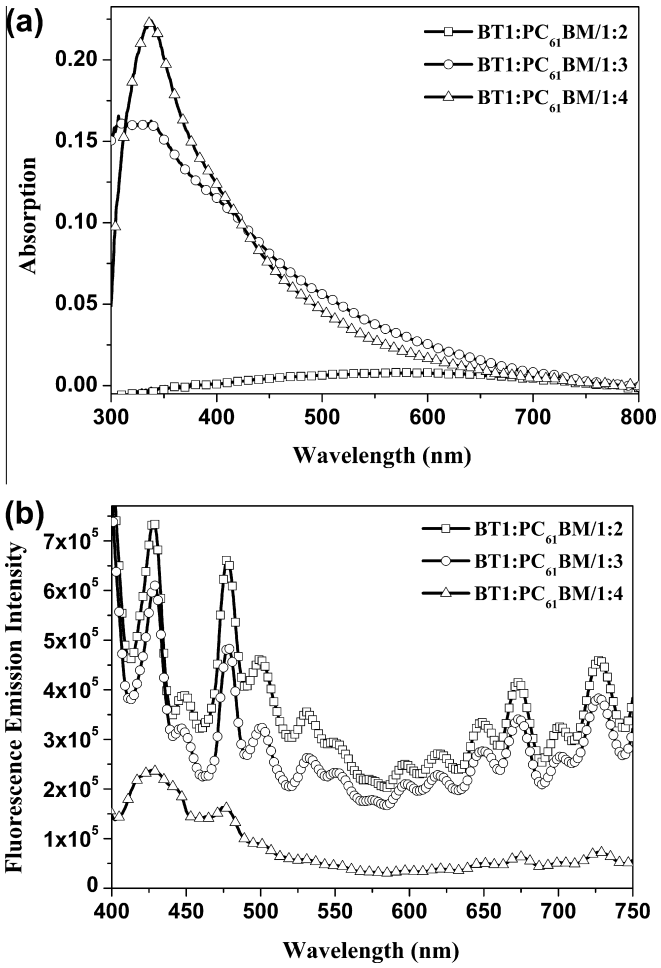

Fig. 6. (a) Electronic absorption and (b) fluorescence emission spectra for **BT1** dye blended with different weight ratios of $PC_{61}BM$ on thin films (λ_{exc} = 385 nm).

P3HT:$PC_{61}BM$ blend, we have first blended the **BT1** dye with different weight ratios of $PC_{61}BM$. Fig. 6a illustrates the UV–vis absorption spectra of thin films for **BT1** dye blended with fullerene at weight ratios of BT1:$PC_{61}BM$ (1:2, 1:3, 1:4 w/w). When **BT1** amount is increased from 20 to 25 wt%, $PC_{61}BM$ absorption enhances in the visible region around 500–700 nm because of the contribution of **BT1** dye absorption to the overall spectra. In the 33 wt%-**BT1** blend, **BT1** disturbs homogeneity of the films so that we could not obtained good film. Both poor solubility in evaporating solvent and also weak interaction with glass substrate for **BT1** dye causes the inhomogeneity on thin films. When the ratio of **BT1** dye in blend is increased from 20 to 33 wt%, $PC_{61}BM$ emission around 700–750 nm goes upper, as shown in Fig. 6b. These data support the energy/electron transfer from **BT1** to $PC_{61}BM$ and the formation of a CT complex by dipole-dipole interactions. In addition, emission spectra of **BT1-3** dyes are partially overlapped with the absorption spectra of $PC_{61}BM$ acceptor, resulting the efficient energy or electron transfer process from the dyes to the $PC_{61}BM$. Fig. 7a shows the absorption spectra for P3HT:BT1:$PC_{61}BM$ ternary system with different weight ratios of P3HT and **BT1** additive. Also, corresponding emission spectra is illustrated in Fig. 7b. Absorption spectrum of P3HT:$PC_{61}BM$ does not significantly change if P3HT content is reduced from 40 to 35 wt% in the blend. In the 10 wt%-**BT1** blend, the emission signal at 550 nm is about half of that in the 5 wt%-**BT1** blend in agreement with the CT process from **BT1** to $PC_{61}BM$ at the excitation wavelength of 450 nm. However, enhancement of emission intensity at 550 nm with the addition of **BT1** dye 15 wt% is not explained by CT process between **BT1** and $PC_{61}BM$. This is attributed to the partially energy or electron transfer process from P3HT to **BT1** in which this quenching is accompanied by a small enhancement of $PC_{61}BM$ emission around 700–750 nm.

Fig. 8a and b show the electronic absorption and emission spectra of P3HT:BT1-3 (1:1 w/w) weight ratio at the excitation wavelength of 385 nm in which both excites **BT1-3** dye and P3HT polymer. In the presence of **BT1** dye, the absorption value of P3HT is improved between 350 and 420 nm by the contribution of light absorbed by **BT1** additive. In the 50 wt%-**BT1** blend, P3HT emission signal is reduced to half value of that in the absence of **BT1** additive and also the maximum of the signal slightly shifted to the blue region. Emission intensity of **BT1** additive appears around 500 nm. These observations may be explained by CT or energy transfer possibility from P3HT to **BT1** dye at this excitation wavelength. P3HT and **BT2** emissions are overlapped and P3HT:BT2 (1:1 w/w) blend gives a combined emission spectra around 650 nm. It is difficult to understand the decrease in P3HT emission intensity. In the 50 wt%-**BT3** blend, P3HT emission decreases less than that of **BT1** addition. This is a good hint that **BT1** dye is more effectively encourage the CT process than that of **BT3** dye in the blend. Also, the highest LUMO energy level of **BT1** dye at −3.04 eV supports the most favorable CT possibility from P3HT to the dye.

Table 3
Cyclic voltammetry data and molecular orbital energies of **BT1-3** compounds with respect to the vacuum level.

Dye	E^0_{red2} (V)	E^0_{red1} (V)	E^0_{ox1} (V)	E^0_{ox2} (V)	LUMO-1 (eV)	LUMO (eV)	HOMO (eV)	HOMO-1 (eV)	E_{gap}[a] (eV)
BT1	−1.45	−1.21	1.71	1.82	−2.80	−3.04	−5.84	−6.07	2.80
BT2	−1.78	−1.17	1.02	–	−2.47	−3.08	−5.59	–	2.51
BT3	–	−1.2	1.35	1.55	–	−3.05	−5.70	−5.80	2.65

[a] E_{gap} values were calculated from the onset values of the visible spectra of the dyes.

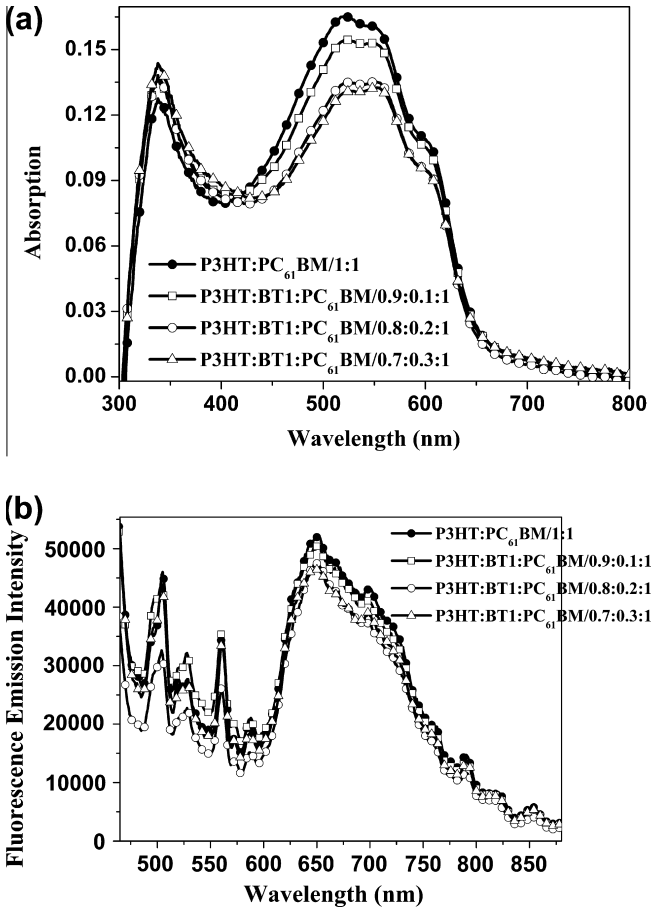

Fig. 7. (a) Electronic absorption and (b) fluorescence emission spectra for P3HT:PC_{61}BM active layer blended with different weight ratios of **BT1** dye on thin films (λ_{exc} = 450 nm).

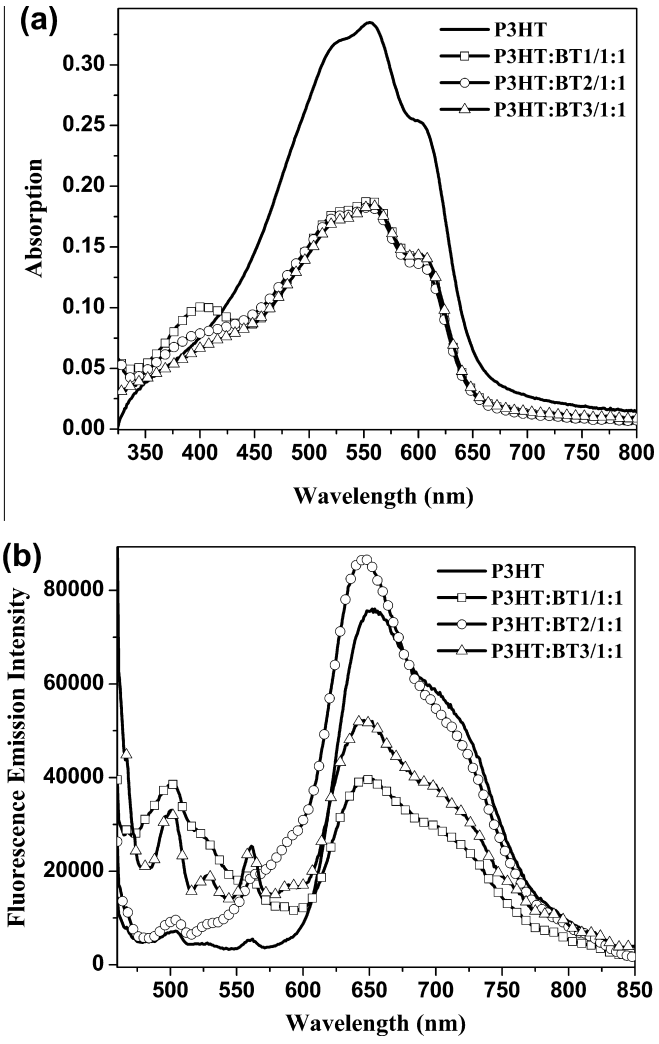

Fig. 8. (a) Electronic absorption (light-colored symbol) and (b) fluorescence emission (dark-colored symbol) spectra for pristine P3HT and blended films of P3HT:BT1-3 (1:1, w/w) active layer (λ_{exc} = 385 nm).

Single photon timing measurements data for P3HT:BT1:PC_{61}BM (0.7:0.3:1, w/w) and P3HT:BT1 (1:1, w/w) on thin film state at different collected emission wavelengths are illustrated in Fig. 9 and also summarized in Table 4. The fluorescence relaxation at all detection wavelengths is clearly monoexponential except the blends for P3HT/**BT2** or **BT3**. When the content of **BT1** additive is increased in ternary blend, fluorescence decay times increase. In the 15 wt%-**BT1** blend, this value reaches to 2.74 ns which is very close to fluorescence decay for control group of pristine P3HT/PC_{61}BM (2.70 ns). The fluorescence decay times strongly depend on the composition of the polymer/fullerene blends [35]. In this case, weight fraction of **BT1** dye is optimum level in the blend to form a homogeneous spatial distribution which is important in exciton quenching at the P3HT/PC_{61}BM interface.

In both blend given in Fig. 10a and b, the higher the emission wavelength of detected signal, the less rapid the decay in fluorescence intensity, excluding at 580 nm. This observation indicates a dynamic fluorescence band shift [50]. Emission intensity is minimal value at the collected emission wavelength of 580 nm. The shortest decay times detected at 480 nm indicate the best nanocomposition in the blend to achieve the largest quenching surface.

Fig. 11 displays the representative illustration of ternary OPV device used in this study with appropriate HOMO and LUMO energy levels. Positions of electronic energy levels for **BT1** structure are suitable with respect to those of P3HT and PC_{61}BM to enject charge transfer. The HOMO level of **BT1** is located between P3HT and PC_{61}BM and similar to LUMO energy levels. Thus, the

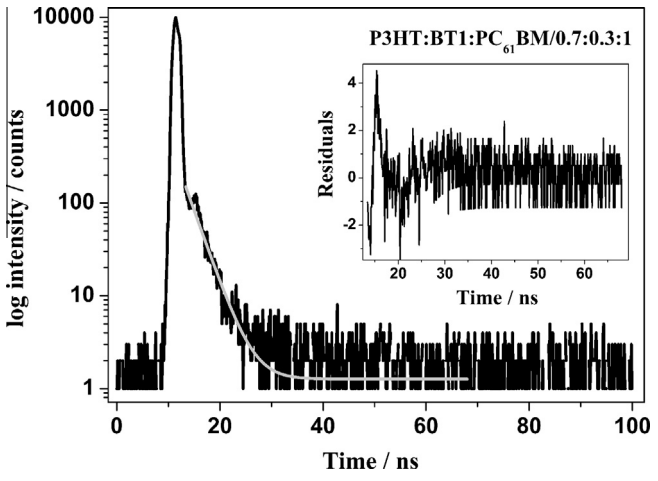

Fig. 9. Fluorescence decay of ternary blend for P3HT:BT1:PC_{61}BM (0.7:0.3:1, w/w) on film state ($\lambda_{detection}$ = 650 nm, time increment = 98 ps).

Table 4
Fluorescence decay times ($\tau_{f(i)}$ (ns)) of **BT1-3** dyes on thin film states (λ_{exc} = 472 nm, $\lambda_{det.}$ = 500 nm for **BT1-3** and BT1: $PC_{61}BM$ layers, and 650 nm for other layers).

Active layer		χ^2	$\tau_{f(1)}$	$\tau_{f(2)}$
Donor:Acceptor	w:w			
BT1	1	1.16	4.62	–
BT2	1	1.22	2.61	–
BT3	1	0.84	2.24	–
BT1:$PC_{61}BM$	1:1	1.07	2.47	–
BT1:$PC_{61}BM$	1:2	0.93	2.18	–
BT1:$PC_{61}BM$	1:3	0.98	2.34	–
BT1:$PC_{61}BM$	1:4	1.15	2.44	–
P3HT	1	0.85	0.85	–
P3HT:$PC_{61}BM$	1:1	1.00	2.70	–
P3HT: BT1:$PC_{61}BM$	0.9:0.1:1	1.26	2.48	–
P3HT: BT1:$PC_{61}BM$	0.8:0.2:1	1.13	2.62	–
P3HT: BT1:$PC_{61}BM$	0.7:0.3:1	1.19	2.74	–
P3HT: BT1	1:1	0.81	2.36	–
P3HT: BT2	1:1	0.88	1.86	6.19
P3HT: BT3	1:1	0.80	0.25	2.21

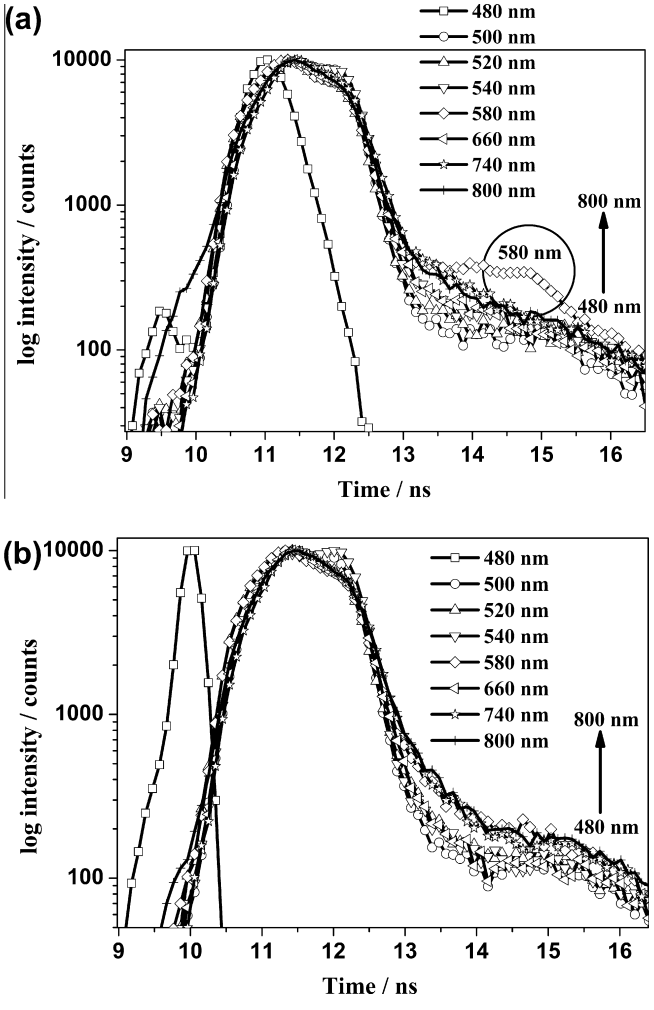

Fig. 10. Fluorescence decays for (a) ternary blend of P3HT:BT1:$PC_{61}BM$ (0.7:0.3:1, w/w) and (b) P3HT:BT1 (1:1, w/w) on film state at different collected emission wavelengths.

transfer of any kind of charge located on **BT1** to the P3HT/$PC_{61}BM$ matrix is energetically favoured.

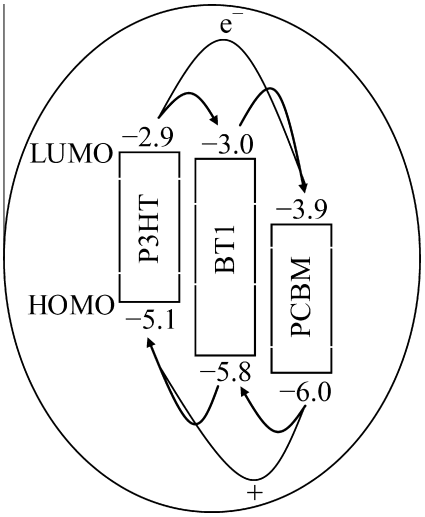

Fig. 11. Representative illustration of ternary OPV device structure with experimentally calculated HOMO and LUMO energy band values for **BT1** dye.

4. Conclusion

We have synthesized and characterized the three BTD derivatives carrying with different donor units. Large shifts of the emission spectra to longer wavelengths in different solvents of polarities are explained by the formation of CT complex between the donor (aniline) and acceptor (BTD) sites of the molecules. CT or energy transfer possibilities from **BT1-3** to $PC_{61}BM$ and from P3HT to **BT1-3** were illustrated by changes in their emission intensities. **BT1** dye is found as the most suitable dye for CT process from P3HT to the dye. Finally, the most suitable weight fraction of **BT1** dye (15 wt%) is chosen in the blend by decay time measurements to form a homogeneous spatial distribution at the P3HT/$PC_{61}BM$ interface. In the following study, P3HT/$PC_{61}BM$ cell performances will be investigated in detail adding **BT1-3** dopants to improve the cell efficiencies compared to control cell.

Acknowledgement

Financial support for this work was provided by the Research Council of Celal Bayar with the project number of 2010-050.

References

[1] D. Muhlbacher, M. Scharber, M. Morana, Z.G. Zhu, D. Waller, R. Gaudiana, C. Brabec, Adv. Mater. 18 (2006) 2884–2889.
[2] M. Koppe, H.-J. Egelhaaf, G. Dennler, M.C. Scharber, C.J. Brabec, P. Schilinsky, C.N. Hoth, Adv. Funct. Mater. 20 (2010) 338–346.
[3] S.H. Park, A. Roy, S. Beaupre, S. Cho, N. Coates, J.S. Moon, D. Moses, M. Leclerc, K. Lee, A.J. Heeger, Nat. Photonics 3 (2009) 297–303.
[4] Y.M. Sun, C.J. Takacs, S.R. Cowan, J.H. Seo, X. Gong, A. Roy, A.J. Heeger, Adv. Mater. 23 (2011) 2226–2230.
[5] B.A.D. Neto, A.A.M. Lapis, E.N. da Silva Júnior, J. Dupont, Eur. J. Org. Chem. 2013 (2013) 228–255.
[6] F. Liang, J. Lu, J. Ding, R. Movileanu, Y. Tao, Macromolecules 42 (2009) 6107–6114.
[7] B. Lim, J. Jo, D. Khim, H.-G. Jeong, B.-K. Yu, J. Kim, D.-Y. Kim, Org. Electron. 11 (2010) 1772–1778.
[8] M. Karakus, D.H. Apaydın, D.E. Yıldız, L. Toppare, A. Cirpan, Polymer 53 (2012) 1198.
[9] K. Ranjith, S.K. Swathi, P. Kumar, P.C. Ramamurthy, Sol. Energy Mater. Sol. Cells 98 (2012) 448–454.
[10] K. Ranjith, S.K. Swathi, A. Malavika, P.C. Ramamurthy, Sol. Energy Mater. Sol. Cells 105 (2012) 263–271.
[11] T. Yasuda, Y. Shinohara, T. Ishi-i, L. Han, Org. Electron. 13 (2012) 1802–1808.
[12] Y. Chen, M. Elshobaki, Z. Ye, J.M. Park, M.A. Noack, K.M. Ho, S. Chaudhary, Phys. Chem. Chem. Phys. 15 (2013) 4297–4302.
[13] K.-H. Ong, S.-L. Lim, J. Li, H.-K. Wong, H.-S. Tan, T.-T. Lin, L.C.H. Moh, J.C. de Mello, Z.-K. Chen, Polym. Chem. 4 (2013) 1863–1873.

[14] E. Bundgaard, F.C. Krebs, Macromol. 39 (2006) 2823–2831.
[15] E. Bundgaard, S.E. Shaheen, F.C. Krebs, D.S. Ginley, Sol. Energy Mater. Sol. Cells 91 (2007) 1631–1637.
[16] M.T. Lloyd, J.E. Anthony, G.G. Malliaras, Mater. Today 10 (2007) 34–41.
[17] W. Li, C. Du, F. Li, Y. Zhou, M. Fahlman, Z. Bo, F. Zhang, Chem. Mater. 21 (2009) 5327–5334.
[18] J.A. Mikroyannidis, M.M. Stylianakis, P. Suresh, P. Balraju, G.D. Sharma, Org. Electron. 10 (2009) 1320–1333.
[19] M. Sun, L. Wang, Y. Cao, Synt. Met. 159 (2009) 556–560.
[20] J. Ah Kong, E. Lim, K.K. Lee, S. Lee, S. Hyun Kim, Sol. Energy Mater. Sol. Cells 94 (2010) 2057–2063.
[21] Z. Wu, B. Fan, F. Xue, C. Adachi, J. Ouyang, Sol. Energy Mater. Sol. Cells 94 (2010) 2230–2237.
[22] J.T. Bloking, X. Han, A.T. Higgs, J.P. Kastrop, L. Pandey, J.E. Norton, C. Risko, C.E. Chen, J.-L. Brédas, M.D. McGehee, A. Sellinger, Chem. Mater. 23 (2011) 5484–5490.
[23] D. Deng, Y. Yang, J. Zhang, C. He, M. Zhang, Z.-G. Zhang, Z. Zhang, Y. Li, Org. Electron. 12 (2011) 614–622.
[24] H. Shang, H. Fan, Y. Liu, W. Hu, Y. Li, X. Zhan, Adv. Mater. 23 (2011) 1554–1557.
[25] N. Cho, K. Song, J.K. Lee, J. Ko, Chem. A Eur. J. 18 (2012) 11433–11439.
[26] P. Dutta, J. Kim, S.H. Eom, W.H. Lee, I.N. Kang, S.H. Lee, ACS Appl. Mater. Interfaces 4 (2012) 6669–6675.
[27] S. Paek, N. Cho, K. Song, M.-J. Jun, J.K. Lee, J. Ko, J. Phys. Chem. C 116 (2012) 23205–23213.
[28] Y.-C. Chen, C.-Y. Hsu, C.-Y. Ho, Y.-T. Tao, J.T. Lin, Org. Electron. 14 (2013) 2290–2298.
[29] S. Zeng, L. Yin, C. Ji, X. Jiang, K. Li, Y. Li, Y. Wang, Chem. Commun. 48 (2012) 10627–10629.
[30] S.-W. Chang, H. Waters, J. Kettle, M. Horie, Org. Electron. 13 (2012) 2967–2974.
[31] A. Ruseckas, P.E. Shaw, I.D.W. Samuel, Dalton Trans. 45 (2009) 10040–10043.
[32] P.E. Shaw, A. Ruseckas, I.D.W. Samuel, Adv. Mater. 20 (2008) 3516–3520.
[33] A.R.S. Kandada, G. Grancini, A. Petrozza, S. Perissinotto, D. Fazzi, S.S.K. Raavi, G. Lanzani, Sci. Rep. 3 (2013) 1–7.
[34] S. van Bavel, E. Sourty, G. de With, K. Frolic, J. Loos, Macromolecules 42 (2009) 7396–7403.
[35] O.V. Mikhnenko, H. Azimi, M. Scharber, M. Morana, P.W.M. Blom, M.A. Loi, Energy Environ. Sci. 5 (2012) 6960–6965.
[36] A.J. Ward, A. Ruseckas, I.D.W. Samuel, J. Phys. Chem. C 116 (2012) 23931–23937.
[37] J.R. Knutson, J.M. Beechem, L. Brand, Chem. Phys. Lett. 102 (1983) 501–507.
[38] J. Pommerehne, H. Vestweber, W. Guss, R.F. Mahrt, H. Bassler, M. Porsch, J. Daub, Adv. Mater. 7 (1995) 551–554.
[39] B.A.D. Neto, A.S.A. Lopes, G. Ebeling, R.S. Goncalves, V.E.U. Costa, F.H. Quina, J. Dupont, Tetrahedron 61 (2005) 10975–10982.
[40] S. Kato, T. Matsumoto, M. Shigeiwa, H. Gorohmaru, S. Maeda, T. Ishi-i, S. Mataka, Chem. Eur. J. 12 (2006) 2303–2317.
[41] R.C. Coffin, J. Peet, J. Rogers, G.C. Bazan, Nature Chem. 1 (2009) 657–661.
[42] A. Leliege, P. Blanchard, T. Rousseau, J. Roncali, Org. Lett. 13 (2011) 3098–3101.
[43] J.W. Eastman, Quantitative Spectrofluorimetry-The Fluorescence Quantum Yield of Quinine Sulfate, Pergamon, Great Britain, 1967.
[44] A.S.D. Sandanayaka, K. Matsukawa, T. Ishi-i, S. Mataka, Y. Araki, O. Ito, J. Phys. Chem. B 108 (2004) 19995–20004.
[45] K.R.J. Thomas, J.T. Lin, M. Velusamy, Y.T. Tao, C.H. Chuen, Adv. Funct. Mater. 14 (2004) 83–90.
[46] J. Pina, J.S. de Melo, D. Breusov, U. Scherf, Phys. Chem. Chem. Phys. 15 (2013) 15204–15213.
[47] M. Maus, R. De, M. Lor, T. Weil, S. Mitra, U.M. Wiesler, A. Herrmann, J. Hofkens, T. Vosch, K. Mullen, F.C. De Schryver, J. Am. Chem. Soc. 123 (2001) 7668–7676.
[48] P. Suppan, Chemistry and Light, The Royal Society of Chemistry, Cambridge, 1994.
[49] V. Ramamurthy, K. Schanze, Organic Photochemistry, Taylor & Francis Group, 2006.
[50] A. Devizis, A. Serbenta, K. Meerholz, D. Hertel, V. Gulbinas, J. Chem. Phys. 133 (2009) 12. 104902-1-7.